VIRTUAL VERSUS REAL NUCLEAR COMPTON SCATTERING IN THE $\Delta(1232)$ REGION

A. Gil, J. A. Gómez Tejedor and E. Oset.

Departamento de Física Teórica and IFIC, Centro Mixto Universidad de Valencia - CSIC, 46100 Burjassot (Valencia) Spain.

Abstract

In this paper we calculate the cross section for Virtual Compton Scattering off nuclei in the delta resonance region. We also calculate the background for the process from Coherent Bremsstrahlung in nuclei and explore the regions where the Virtual Compton Scattering cross section dominates. The study also shows that it is possible to extract the cross section for Real Compton Scattering from the Virtual Compton one in a wide range of scattering angles.

Keywords: Real Compton Scattering in nuclei, Virtual Compton Scattering in nuclei, Coherent Bremsstrahlung in nuclei, delta resonance.

PACs numbers: 24.30.Gd , 25.20.-x , 25.30.-c

1 Introduction

For the last years, Virtual Compton Scattering (VCS) on the nucleon target has attracted much interest from different points of view. For the case of very hard photons it could provide a stringent test of perturbative Quantum Chromo-Dynamics [1], although large experimental difficulties appear. Below pion threshold it allows one to measure new electromagnetic observables which generalize the usual magnetic and electric polarizabilities [2, 3, 4].

For the nuclear target, Virtual Compton Scattering at intermediate energy should be a highly advanced method to study nuclear structure, although no data are available so far, and there is only one theoretical study [5].

On the other hand, for Real Compton Scattering (RCS) much more information is available, both for nucleon and nuclear targets. In the case of a nucleon target, RCS scattering has been experimentally investigated in all energy range: in the low energy limit at Mainz [6], Saskatoon [7] and Illinois [8]; in the resonance region at Bonn [9] and Tokyo [10, 11]; and in the deep inelastic region at Cornell [12, 13] and SLAC [14, 15].

RCS on nuclei has been the subject of several recent theoretical and experimental articles [16]-[29].

In this paper we study the coherent Virtual Compton Scattering in nuclei, $A(e, e'\gamma)A$. In this process the electron emits a virtual photon which is scattered in the nucleus producing a real photon in the final state while the nucleus remain in its ground state.

Apart from the interest by itself, this process could be a useful tool to investigate Real Compton Scattering in nuclei without the need to produce real photons: when the angle between the final and initial electron is very small, the intermediate virtual photon is almost real, and then, we can extract the RCS cross section from the VCS one.

Why could it be interesting to investigate RCS from VCS?. From the experimental point of view, if we analyze both processes (see Fig. 1), one can see that the RCS is a two steps process: First, the electron is scattered in a nucleus in order to produce a real photon from Bremsstrahlung (this process is of order $Z^2\alpha^3$), and second, this real photon is scattered in a second nucleus in order to produce the RCS (this is an order $(A\alpha)^2$ process); in total, this process is of order $Z^2\alpha^5A^2$. On the other hand, the VCS is a one step process: the electron exchanges a virtual photon with the nucleus, and a real photon is emitted; this process is of order $\alpha(A\alpha)^2$. Therefore, in principle, the ratio between RCS and VCS should be around $Z^2\alpha^2$, smaller than 0.1 for most nuclei. However, this is still a large overestimate since the involvement of two targets in the real photon case, limits largely the final counts. Then, in principle, it should be much more efficient to perform an experiment for VCS than for RCS. However, from the experimental point of view, dealing with electrons comport additional difficulties with respect to photons. One of the most important difficulties is the large background that

one would encounter coming from the Coherent Bremsstrahlung (CB) in nuclei: in this process the real photon is emitted from the electron, not from the nucleus. Thus, we have also studied this process in order to determine the experimental accessible regions, where the signal for the VCS is clearly visible.

We have concentrated our study around the peak of the $\Delta(1232)$ resonance region, i.e., when the energy of the virtual photon is equal to 340 MeV.

We have performed calculations for ^{12}C and ^{40}Ca at electron energies accessible at Mainz and TJNAF.

2 Virtual Compton Scattering in nuclei.

The differential cross section for the VCS in nuclei (see Fig. 2) in the LAB system is given by:

$$\frac{d^5\sigma}{d\Omega_{e'}d\Omega_\gamma d\omega'} = \frac{m_e^2}{2(2\pi)^5}\,\frac{M}{E'_A}\,\frac{|\vec{k}'|\omega'}{|\vec{k}|}\,\bar{\Sigma}\Sigma|\mathcal{M}|^2 \tag{1}$$

where, $k = (E, \vec{k})$ and $k' = (E', \vec{k})$ are the four-momenta of the incoming at outgoing electron respectively; $q = (\omega, \vec{q})$ and $q' = (\omega', \vec{q}\,')$ are the four-momenta of the intermediate and final photon respectively; $p = (M, \vec{0}\,)$ and $p' = (E'_A, \vec{p}\,')$ are the momenta of the initial and final nucleus; m_e is the electron mass; $\mathcal{M}$ is the amplitude of the process. As we consider the unpolarized cross section, we sum over final states and average over initial ones.

The amplitude $\mathcal{M}$ is given by:

$$\mathcal{M} = \frac{e}{q^2}\bar{u}_{r'}(k')\gamma^\mu u_r(k)\tilde{\Pi}_{\mu\nu}(q,q')\varepsilon^\nu(q') \tag{2}$$

in this expression $u_r(k)(u_{r'}(k'))$ are the Dirac spinors for the initial (and final) electron with spin $r(r')$; $\varepsilon^\nu(q')$ is the vector polarization of the final photon; $\tilde{\Pi}_{\mu\nu}(q,q')$ is the hadronic current. In the delta region where we are interested in, and for spin saturated nuclei, this hadronic part of the amplitude is dominated by the contribution of the $\Delta(1232)$ [27, 26, 31], and it is given by [26]:

$$-i\tilde{\Pi}^{\mu\nu}_\Delta(q,q') = \sum_{M_s}\sum_{M_I}(-iT^\mu(q))(-iT^{\dagger\nu}(q'))\int d^3r\, e^{i(\vec{q}-\vec{q}\,')\cdot\vec{r}} \tag{3}$$

$$\frac{1}{4}\frac{\rho(\vec{r}\,)}{\sqrt{s_\Delta} - m_\Delta + i\dfrac{\tilde{\Gamma}(\sqrt{s_\Delta},\rho(\vec{r}\,))}{2} - \sum_\Delta(\sqrt{s_\Delta},\rho(\vec{r}\,))}$$

in this expression, $\rho(\vec{r}\,)$ is the nuclear density, for which we use a two Fermi parameters parametrization [30]; $\sqrt{s_\Delta}$ is the invariant mass of the nucleon-photon system. In order to calculate this invariant mass, we assume for the initial nucleon an average momentum given by:

$$\vec{p} = (\vec{q}' - \vec{q})/2 \tag{4}$$

used also in [27, 5, 26]. $\tilde{\Gamma}(\sqrt{s_\Delta}, \rho(\vec{r}))$ is the $\Delta(1232)$ width corrected by Pauli blocking [33]. $\Sigma_\Delta(\sqrt{s_\Delta}, \rho(\vec{r}))$ is the Δ self-energy which includes quasielastic, plus two-body and three-body contributions related to photon absorption[33, 34]. $T^\mu(q)$ is the $\gamma N\Delta$ vertex, which, in the C. M. system of reference is given by:

$$T^\mu(q) = \sqrt{\frac{2}{3}} \frac{f_\gamma}{m_\pi} \frac{\sqrt{s_\Delta}}{m_\Delta} \left\{ \begin{array}{c} 0 \\ \vec{S} \times \vec{q} \end{array} \right\} \tag{5}$$

where the factor $\sqrt{\frac{2}{3}}$ came from isospin, $f_\gamma = 0.12$ is the $\gamma N\Delta$ coupling constant [31, 32], and $\vec{S}$ is the 1/2 to 3/2 transition spin operator normalized as:

$$< \frac{3}{2}, M \, |S^\dagger_\nu| \, \frac{1}{2}, m >= \mathcal{C} \left(\frac{1}{2} \, 1 \, \frac{3}{2}; m, \nu, M \right) \tag{6}$$

3 Background: Coherent Bremsstrahlung in nuclei.

As we already said, photon emission from CB can be very important, depending on the kinematics. In this process the nucleus acts as a momentum source (with no energy transfer) and the photon is emitted from the electron. The cross section for this process in the one photon exchange approximation is given by [35]:

$$\frac{d^5\omega}{d\Omega_{e'} \Omega_\gamma d\omega'} = \frac{m_e^2}{2(2\pi)^5} e^4 \frac{\omega' |\vec{k}'|}{|\vec{k}|} L^{\mu\nu} A_\mu(\vec{q}) A_\nu(\vec{q}) \tag{7}$$

with $L^{\mu\nu}$ the leptonic tensor for the process (detailed expressions can be found in ref. [35]); $A_\mu(\vec{q})$ the Coulomb potential in momentum space, which is the Fourier transform of the Coulomb potential in coordinate space,

$$A^\mu(\vec{x}) = (A^0(\vec{x}), \vec{0}) = \left(\frac{Ze}{4\pi} \int d^3x' \frac{\rho_p(x')}{|\vec{x} - \vec{x}'|} \, , \, \vec{0} \right). \tag{8}$$

In order to calculate the total cross section for $A(e, e'\gamma)A$ we include also the interference between this process and the VCS.

4 Real Compton Scattering.

In this section we compare VCS and RCS in order to see if it is possible to extract the later from the first one.

The cross section for the RCS process (see Fig. 4) in the LAB system is given by [26]:

$$\left(\frac{d\sigma}{d\Omega_\gamma}\right)_{\rm real} = \frac{1}{16\pi^2}\,|\mathcal{M}(\vec{q},\vec{q}\,')|^2. \tag{9}$$

Once again, we are interested on the Δ resonance region. Then, the amplitude $\mathcal{M}$ is given by:

$$\mathcal{M}(\vec{q},\vec{q}\,') = \tilde{\Pi}^{\mu\nu}_{\Delta}(\vec{q},\vec{q}\,')\varepsilon_\mu(\vec{q})\varepsilon_\nu(\vec{q}\,') \tag{10}$$

Now, in order to compare this cross section to the VCS one, we write down the cross section for unpolarized photon production in (e,e') reactions [36]:

$$\frac{d^5\sigma}{d\Omega_{e'}d\omega' d\Omega_\gamma} = \Gamma\left\{\frac{d\sigma_T}{d\Omega_\gamma} + \epsilon\frac{d\sigma_L}{d\Omega_\gamma} + \right.$$

$$\left. + \epsilon\,\frac{d\sigma_p}{d\Omega_\gamma}\,cos2\phi_\gamma + \sqrt{2\epsilon(1+\epsilon)}\,\frac{d\sigma_I}{d\Omega_\gamma}\,cos\phi_\gamma\,\right\} \tag{11}$$

where

$$\Gamma = \frac{\alpha}{2\pi^2}\frac{1}{-q^2}\frac{|\vec{k}'|}{|\vec{k}|}\frac{1}{1-\epsilon}k_\gamma \tag{12}$$

$$\epsilon = \left(1 - \frac{2\vec{q}^{\,2}}{q^2}\tan^2(\theta/2)\right)^{-1}$$

$$k_\gamma = \frac{s-M^2}{2M}$$

In the $\Delta(1232)$ region, the cross section for the VCS is dominated by the transverse part [5]:

$$\frac{d^5\sigma}{d\Omega_{e'}d\omega' d\Omega_\gamma} \simeq \Gamma\frac{d\sigma_T}{d\Omega_\gamma} \tag{13}$$

and for small angles between the final and initial electrons, the intermediate virtual photon is almost real and then,

$$\frac{d\sigma_T}{d\Omega_\gamma} \simeq \left(\frac{d\sigma}{d\Omega_\gamma}\right)_{\rm real} \tag{14}$$

Then, in principle, it is possible to extract the RCS cross section from the VCS one. We will see in the results section how good this approximation is. In order to compare both processes the energy of the incoming photon in the RCS is taken as $q^0 = 340\,MeV$ (the same value than in the VCS for the intermediate photon), but then $q = q^0$ unlike for the VCS case.

5 Results.

5.1 Virtual Compton scattering compared to the background (Coherent Bremsstrahlung).

In Figs. 5-10 we show the differential cross section for VCS (dotted lines), compared to the background (dashed lines), as well as the coherent sum of both processes (solid lines). We have done such calculations for ^{12}C and ^{40}Ca for different angles between the final and initial electron, $\theta_{e'}^{LAB}$, ($\theta_{e'}^{LAB} = 2, 5, 10, 15$ degrees), and for different energies of the incoming electron, E_e, ($E_e = 500, 800$ and $2000\, MeV$), keeping always the energy of the intermediate photon equal to $340\, MeV$, in order to be always in the delta resonance region. We have plotted the differential cross section as a function of the angle between the final photon and the intermediate photon in the LAB system (θ_{γ}^{LAB}). We have integrated over the angle ϕ_{γ} of the photon.

As a first impression, we can see in Figs. 5-10 that the cross section for both processes decreases when one increases the angle of the outgoing electron, $\theta_{e'}^{LAB}$, and also when we increase the energy of the incoming electron, E_e. Then, we can first conclude that the experimental study of the present process would be favoured by small electron angles, $\theta_{e'}^{LAB}$, and small electron energies, E_e.

In addition, we can see that the behaviour of the cross section is very similar for ^{12}C and ^{40}Ca except by the different nuclear form factor, and the fact that cross sections depend on A^2, and then, the cross section for ^{40}Ca is larger than for ^{12}C.

Looking more carefully to the cross section, we can see that for $E_e = 500\, MeV$, and for small electron angles ($\theta_{e'}^{LAB} = 2 - 5$ deg.) the VCS dominates the cross section for photon angles larger than $25 - 30$ degrees. For $\theta_{e'}^{LAB} = 10 - 15$ degrees we can see that it is necessary to go to higher photon angles ($\theta_{\gamma}^{LAB} > 40 - 60$ deg.) in order to see the VCS signal over the background. Very similar features appear for $E_e = 800\, MeV$, although here it is necessary to look at higher photon angles in order to measure the VCS.

A different behaviour appears for larger electron energy ($E_e = 2000\ MeV$). In this case, we can see that for very small electron angles $\theta_{e'}^{LAB} = 2$ deg.) it is possible to see the VCS signal over the background for $\theta_{\gamma}^{LAB} > 25$ deg. However if we increase the electron angles it is necessary to go to very high photon angle ($\theta_{\gamma}^{LAB} > 120$ deg. for $\theta_{e'}^{LAB} = 15$ deg.) in order to measure the VCS.

5.2 Virtual Compton Scattering compared to Real Compton Scattering.

In Figs. 11-16 we can see the differential cross section for the RCS (dotted lines) compared to the VCS cross section divided by the factor Γ of Eq. (12) (solid

line), and we have also plotted the transverse part of the cross section, $d\sigma_T/d\Omega_\gamma$ (dashed lines).

The first thing that we can see is that the transverse part of the cross sections for the VCS (dashed line) is almost the same than the total ones (continuous lines): both lines, the continuous one and the dashed line, almost overlapping for all energies.

Comparing now both the VCS and RCS cross sections at $E_e = 500\,MeV$ we see that they are essentially equal at $\theta_e < 15$ deg. If we move to larger electron energies, $E_e = 800\,MeV$ this agreement between both calculations remains good for small electron angles ($\theta_{e'}^{LAB} = 2-5$ deg.), but is not so good for larger electron angles ($\theta_{e'}^{LAB} = 10 - 15$ deg.).

Finally, at $E_e = 2000\,MeV$, only at very small electron angles, ($\theta_{e'}^{LAB} = 2$ deg.), is there agreement between the VCS and RCS cross section and we observe important discrepancies between them for larger electron angles.

Thus, we see that in order to extract the cross section for the RCS from the VCS process it is necessary to measure at small electron energies, and also small electron angles. Even then one can not get the VCS cross sections at angles of the photon smaller than 30 degrees since at small photon angles the Bremsstrahlung background dominates the cross section. This might look like an important limitation of the method, but in practice it is not. The reason is that the forward part of the RCS cross section can be very well reproduced [26, 37] via the optical theorem, from experimental data on the total photonuclear cross section [38, 39] and the real part of the RCS forward amplitude obtained from dispersion relations [40] . Furthermore the fall down of the cross section up to 50-60 degrees is well reproduced in terms of the nuclear form factor. Thus the genuine new information contained in RCS lies precisely in the not very forward angles [41], where in fact there are still discrepancies between theory and experiment [27, 25, 26].

Given the limited amount of data on RCS, and the present persistent discrepancies between theory and experiment, obtaining more data on RCS is an important task. The method derived here can make this goal easier than it has been so far.

6 Conclusions

Our conclusions can be summarized in two main points:

On the first hand, we have studied the VCS cross section in the $\Delta(1232)$ region. We have compared this cross section with the background (coming from the CB) that one would encounter in the implementation of the experiment. We have found the accessible experimental regions. We have seen that for small angles of the outgoing photon the CB dominates the reaction. However, at photon angles around and above 30 deg., it is possible to measure VCS. In addition, we

have seen that the most favourable case happens for small electron energies and small outgoing electron angles. In this case, the VCS cross section is maximum and, although the CB is also maximum, the last one decreases faster than the first one with the outgoing photon angle.

On the second hand, we have compared the VCS cross section with the RCS one. We have seen that for small electron energies and small electron angles it is possible to extract the RCS cross section from the measurement of the VCS one. This is due to the fact that in such conditions ($\theta_{e'}^{LAB}$ small and E_e small), the intermediate virtual photon in the VCS process is almost real, and what we really have in this case is almost real Compton scattering. The present study has, however, quantized how real the photon must be in order to have the VCS and RCS cross sections equal at level of 2-3%. However, we should not forget about the already commented background which would appear in the measurement of VCS and which makes the region of small angles not experimentally accessible. On the other hand we argued that the experimental information on forward Compton scattering is already contained in the existing precise measurements of the total photonuclear cross section. Hence the region of angles which can be explored with the present method is precisely the one offering genuine new information about RCS.

We would like to acknowledge partial support from CICYT contract number AEN 96-1719. One of us, A. Gil, wishes to thank the Conselleria d'Educació de la Generalitat Valenciana for financial support.

References

[1] G. R. Farrar and H. Zhang, Phys. Rev. D41 (1990) 3348.

[2] P. A. M. Guichon, G. Liu, A. W. Thomas, Nucl. Phys. A591 (1995) 606.

[3] G. Audit et al., CEBAF proposal PR-93-050 (1993).

[4] J. Berthot et al., MAMI proposal SW9604 (1995).

[5] B. Pasquini and S. Boffi, preprint nucl-th/9605003.

[6] A. Zieger et al., Phys. Lett B278 (1992) 34.

[7] E. L. Hallin, Phys. Rev. D48 (1993) 1428.

[8] F. J. Federspiel et al., Phys. Rev. Lett. 67 (1991) 1511.

[9] M. Jung et al., Z. Phys. C10 (198).

[10] Y. Wada et al., Nucl. Phys. B247 (1984) 313.

[11] Ishii et al., Nucl. Phys. B254 (1985) 458.

[12] J. Deutsch et al., Phys. Rev. D8 (1973) 3828.

[13] M. A. Shupe et al., Phys. Rev. D19 (1979) 1929.

[14] R. L. Anderson et al., Phys. Rev. Lett. 25 (1970) 1218.

[15] D. O. Caldwell et al., Phys. Rev. Lett. 33 (1974) 868.

[16] M. Schumacher et al., Nucl. Phys. A576 (1994) 603.

[17] G. E. Brown, M. Rho and M. Soyeur, Nucl. Phys. A553 (1993) 705c

[18] W. Weise, Nucl. Phys. A553 (1993) 59c.

[19] A. Baumann et al., Phys. Rev. C35 (1988) 1940.

[20] E. Hayward, B. F. Gibson and J. S. O'Connell, Phys. Rev. C5 (1972) 846.

[21] D. O. Riska, Phys. Rep. 181 (1989) 207.

[22] K. P. Schelhaas et al., Nucl. Phys. A506 (1990) 307.

[23] K. W. Rose et al., Nucl. Phys. A514 (1990) 621.

[24] M. Ludwing et al., Phys. Lett. B274 (1992) 275.

[25] J. H. Koch, E. J. Moniz and N. Ohtsuka, Annals of Phys. 154 (1984) 99.

[26] R. C. Carrasco, Anales de Física, 90 (1994) 8.

[27] B. Pasquini and S. Boffi, Nucl. Phys. A591 (1995) 606.

[28] E. J. Austin et al., Phys. Rev. Lett. 57 (1986) 972.

[29] E. J. Austin et al., Phys. Rev. Lett. 61 (1988) 1922.

[30] H. de Vries, C. W. de Jager and C. de Vries, Atomic data and nuclear data tables, 36, (1987) 495.

[31] R. C. Carrasco and E. Oset, Nucl. Phys. A536 (1992) 445.

[32] F. A. Berends, A. Donachie and D. L. Weaver, Nucl. Phys. 84 (1967) 54; F. A. Berends and A. Donnachie, Nucl. Phys. B84 (1975) 342

[33] E. Oset and L.L. Salcedo, Nucl. Phys. A468 (1987) 631

[34] C. García Recio, E. Oset, L.L. Salcedo, D. Strottman and M.J. López, Nucl. Phys. A526 (1991) 685

[35] See for instance, C. Itzykson and J.B. Zuber, *Quantum Field Theory*, McGraw-Hill, New York, 1980, Section 5-2-4.

[36] E. Amaldi, S. Fubini and G. Furlan, *Pion electroproduction*, Springer Tracts in Modern Physics, Vol. 83 (Springer, Berlin, 1979)

[37] E. J. Austin et al., Phys. Rev. Lett. 57 (1986) 972

[38] J. Ahrens, Nucl. Phys. A335 (1980) 67

[39] P. Carlos et al., Nucl. Phys. A431 (1984) 573

[40] J. Ahrens, L.S. Ferreira and W. Weise, Nucl. Phys. A485 (1988) 621

[41] M. Schumacher, P. Rullhusen and A. Baumann, Nuovo Cimento 100 (1988) 339

Figure captions:

Figure 1: Schematical comparison between Real Compton Scattering and Virtual Compton Scattering.

Figure 2: Diagrammatic representation of the VCS process in nuclei. In the present case one of the hadronic lines in the intermediate states would be a $\Delta(1232)$.

Figure 3: Feynman diagram for the coherent Bremsstrahlung in nuclei.

Figure 4: Diagrammatic representation of the RCS process in nuclei. In the present case one of the hadronic lines in the intermediate states would be a $\Delta(1232)$.

Figure 5: Differential cross section for the VCS process (dotted lines), Coherent Bremsstrahlung (dashed lines) and the total cross section (solid lines) in ^{12}C for different outgoing electron angles ($\theta_{e'}^{LAB} = 2, 5, 10$ and 15 deg.) and for an incoming electron energy, E_e, of $500\,MeV$ as a function of the final photon angle, θ_γ^{LAB} which is the angle between $\vec{q}$ and $\vec{q}\,'$. We always fix the transfer energy $E_e' - E_e$ equal to $340\,MeV$, in order to be around the delta resonance peak.

Figure 6: Same as Figure 5 for $E_e = 800\,MeV$.

Figure 7: Same as Figure 5 for $E_e = 2000\,MeV$.

Figure 8: Same as Figure 5 for ^{40}Ca.

Figure 9: Same as Figure 5 for ^{40}Ca and $E_e = 800\,MeV$.

Figure 10: Same as Figure 5 for ^{40}Ca and $E_e = 2000\,MeV$.

Figure 11: Differential cross section for the RCS process (dotted line), compared to the VCS divided by Γ (solid line) and the transverse part of the VCS cross section (dashed line) in ^{12}C for different outgoing electron angles ($\theta_{e'}^{LAB} = 2, 5, 10$ and 15 deg.) and for an incoming electron energy of $500\,MeV$ as a function of the final photon angle, θ_γ^{LAB}. We always fix the transfer energy $E_e' - E_e$ equal to $340\,MeV$ in order to be around the delta resonance peak.

Figure 12: Same as Figure 11 for $E_e = 800\,MeV$.

Figure 13: Same as Figure 11 for $E_e = 2000\,MeV$.

Figure 14: Same as Figure 11 for ^{40}Ca.

Figure 15: Same as Figure 11 for ^{40}Ca and $E_e = 800\,MeV$.

Figure 16: Same as Figure 12 for ^{40}Ca and $E_e = 2000\,MeV$.

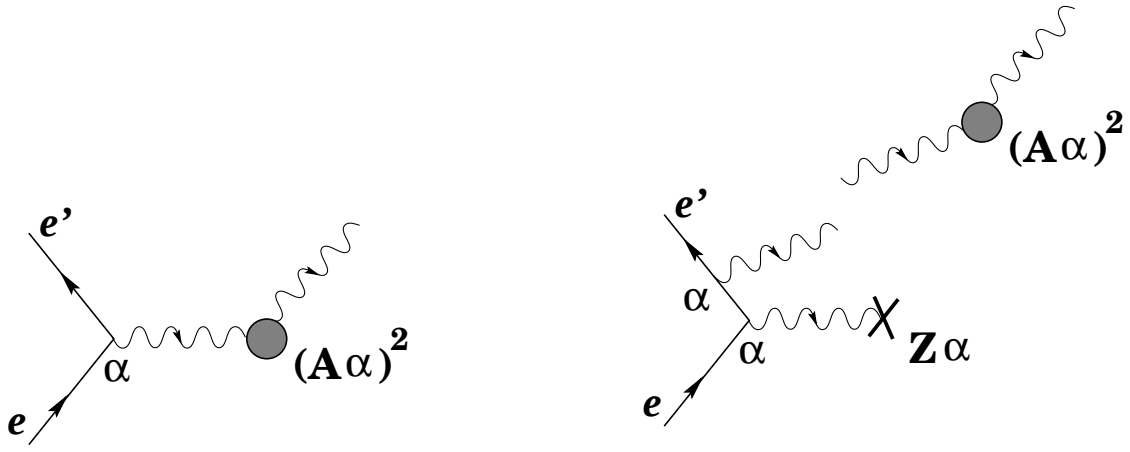

Figure 1:

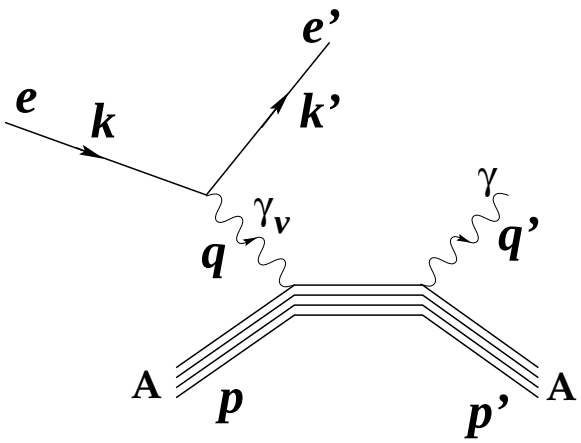

Figure 2:

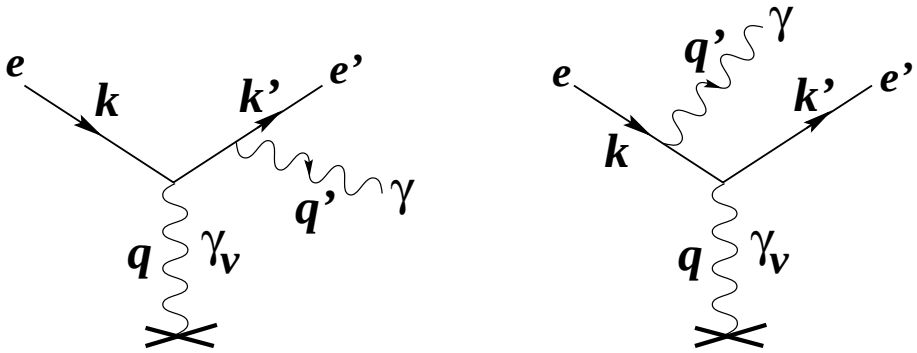

Figure 3:

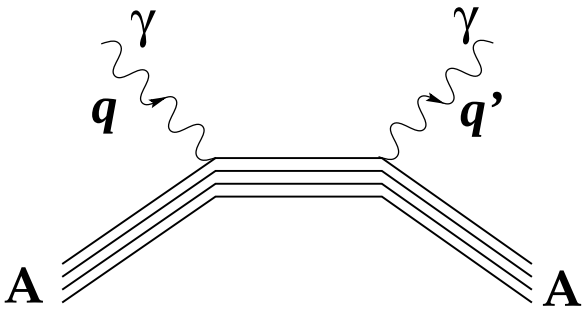

Figure 4:

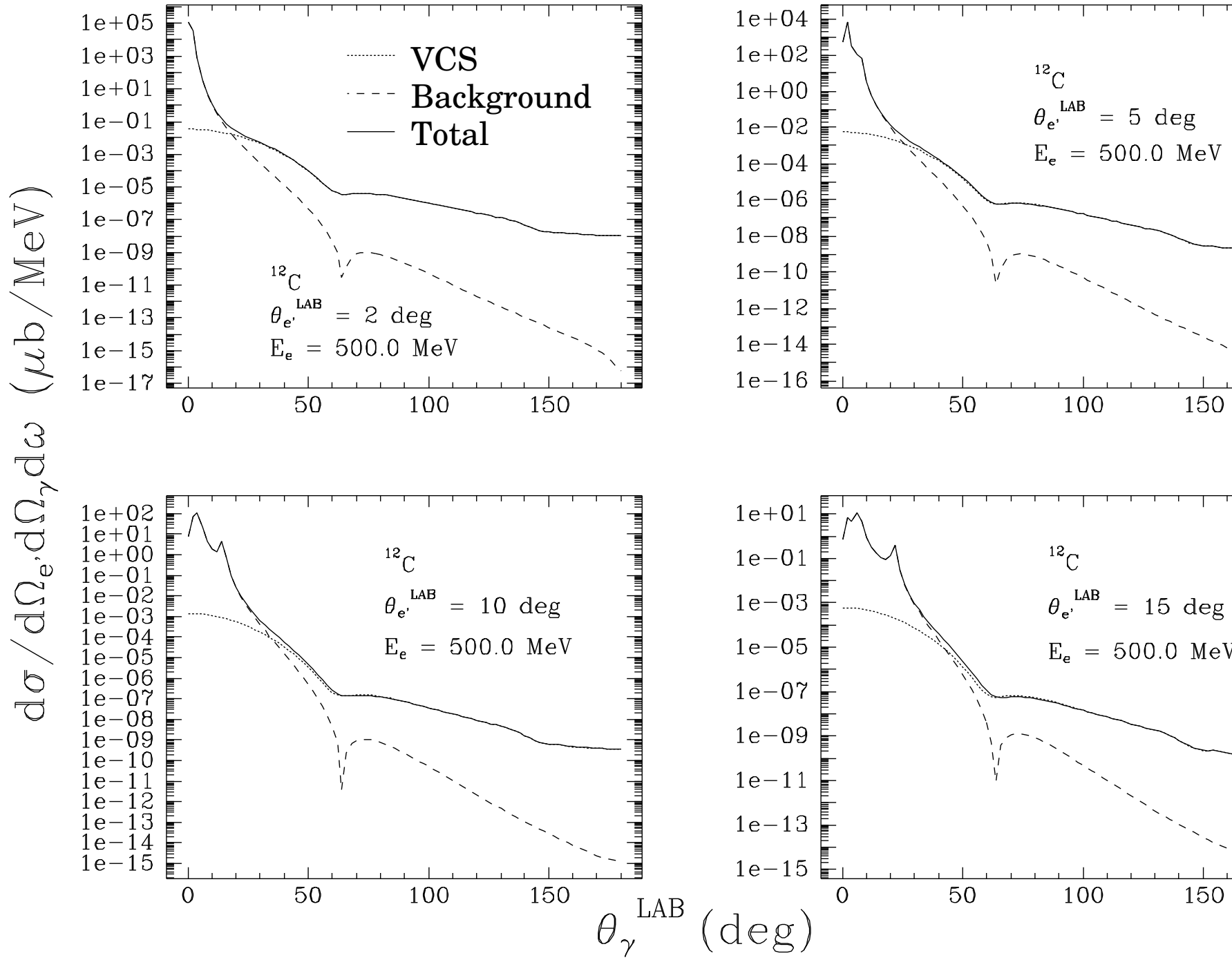
VCS
Background
Total
^{12}C
$\theta_{e'}^{LAB}$ = 2 deg
E_e = 500.0 MeV
^{12}C
$\theta_{e'}^{LAB}$ = 5 deg
E_e = 500.0 MeV
^{12}C
$\theta_{e'}^{LAB}$ = 10 deg
E_e = 500.0 MeV
^{12}C
$\theta_{e'}^{LAB}$ = 15 deg
E_e = 500.0 MeV
$d\sigma / d\Omega_{e'} d\Omega_\gamma d\omega$ (μb/MeV)
θ_γ^{LAB} (deg)

Figure 5:

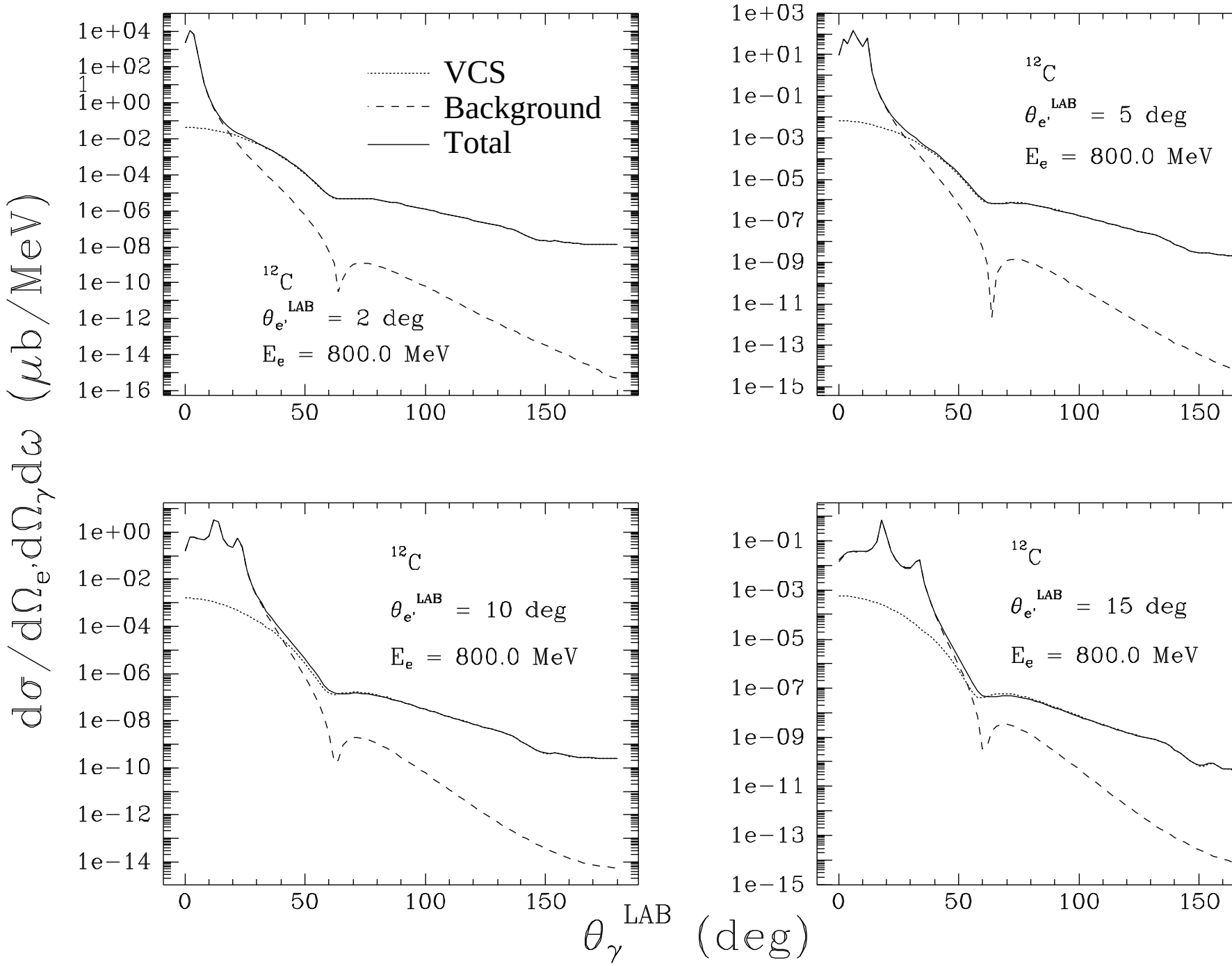
VCS
Background
Total
^{12}C
$\theta_{e'}^{LAB}$ = 2 deg
E_e = 800.0 MeV
^{12}C
$\theta_{e'}^{LAB}$ = 5 deg
E_e = 800.0 MeV
^{12}C
$\theta_{e'}^{LAB}$ = 10 deg
E_e = 800.0 MeV
^{12}C
$\theta_{e'}^{LAB}$ = 15 deg
E_e = 800.0 MeV
$d\sigma/d\Omega_{e'}d\Omega_\gamma d\omega$ (μb/MeV)
θ_γ^{LAB} (deg)

Figure 6:

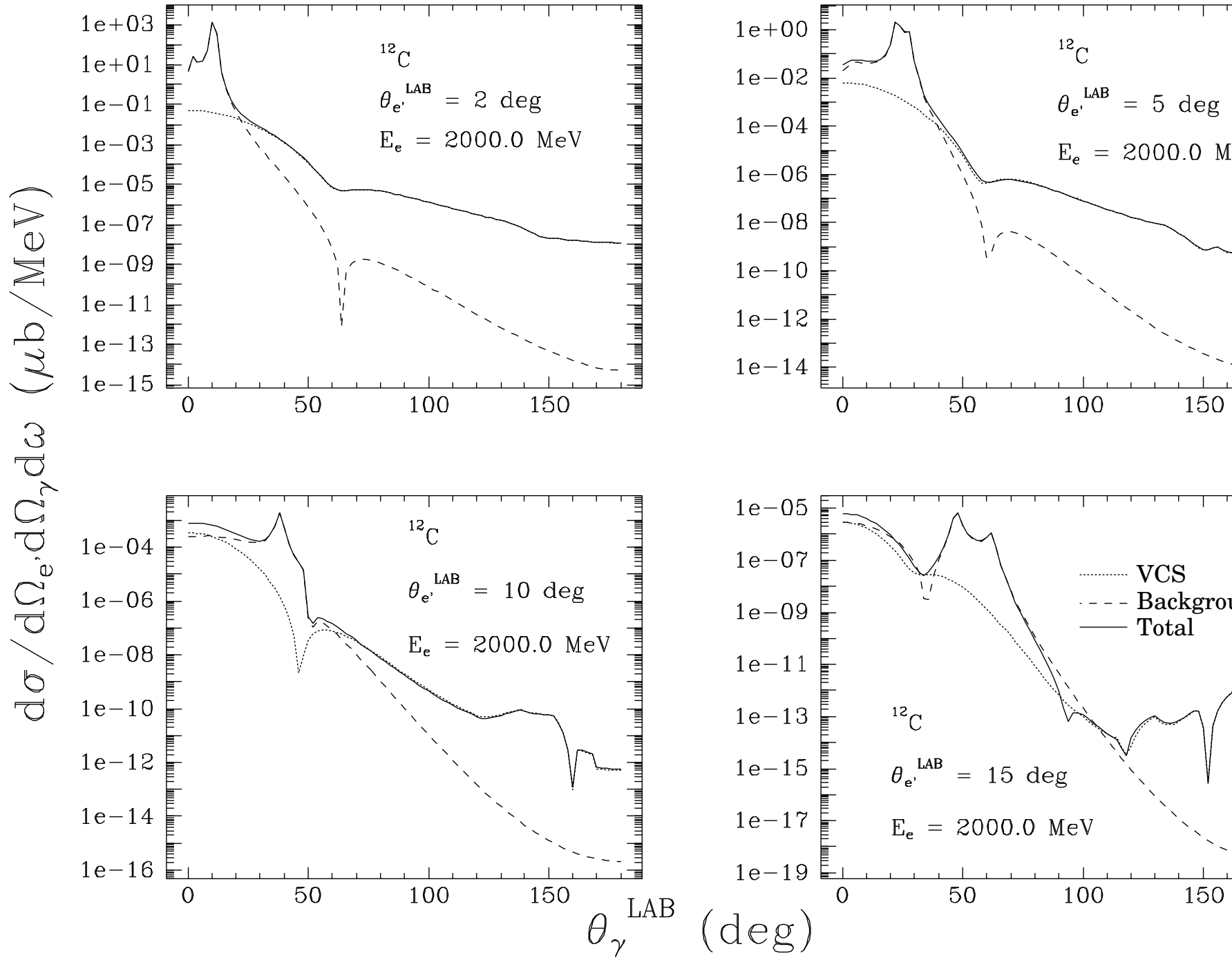
^{12}C
$\theta_{e'}^{LAB}$ = 2 deg
E_e = 2000.0 MeV
^{12}C
$\theta_{e'}^{LAB}$ = 5 deg
E_e = 2000.0 M
^{12}C
$\theta_{e'}^{LAB}$ = 10 deg
E_e = 2000.0 MeV
^{12}C
$\theta_{e'}^{LAB}$ = 15 deg
E_e = 2000.0 MeV
VCS
Backgrou
Total
$d\sigma/d\Omega_{e'}d\Omega_\gamma d\omega$ (μb/MeV)
θ_γ^{LAB} (deg)

Figure 7:

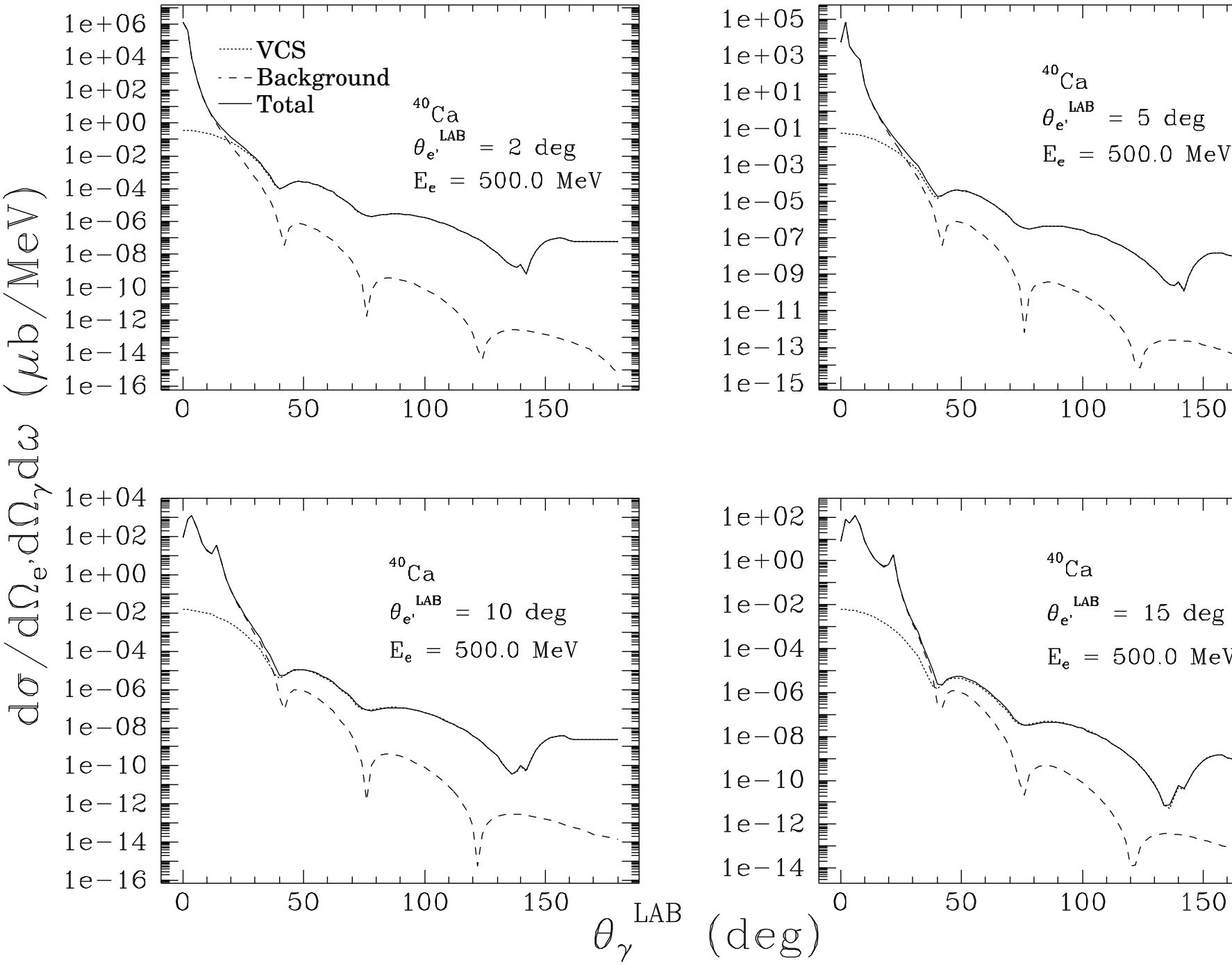
VCS
Background
Total
^{40}Ca
$\theta_{e'}^{LAB}$ = 2 deg
E_e = 500.0 MeV
^{40}Ca
$\theta_{e'}^{LAB}$ = 5 deg
E_e = 500.0 MeV
^{40}Ca
$\theta_{e'}^{LAB}$ = 10 deg
E_e = 500.0 MeV
^{40}Ca
$\theta_{e'}^{LAB}$ = 15 deg
E_e = 500.0 MeV
$d\sigma/d\Omega_{e'}d\Omega_\gamma d\omega$ (μb/MeV)
θ_γ^{LAB} (deg)

Figure 8:

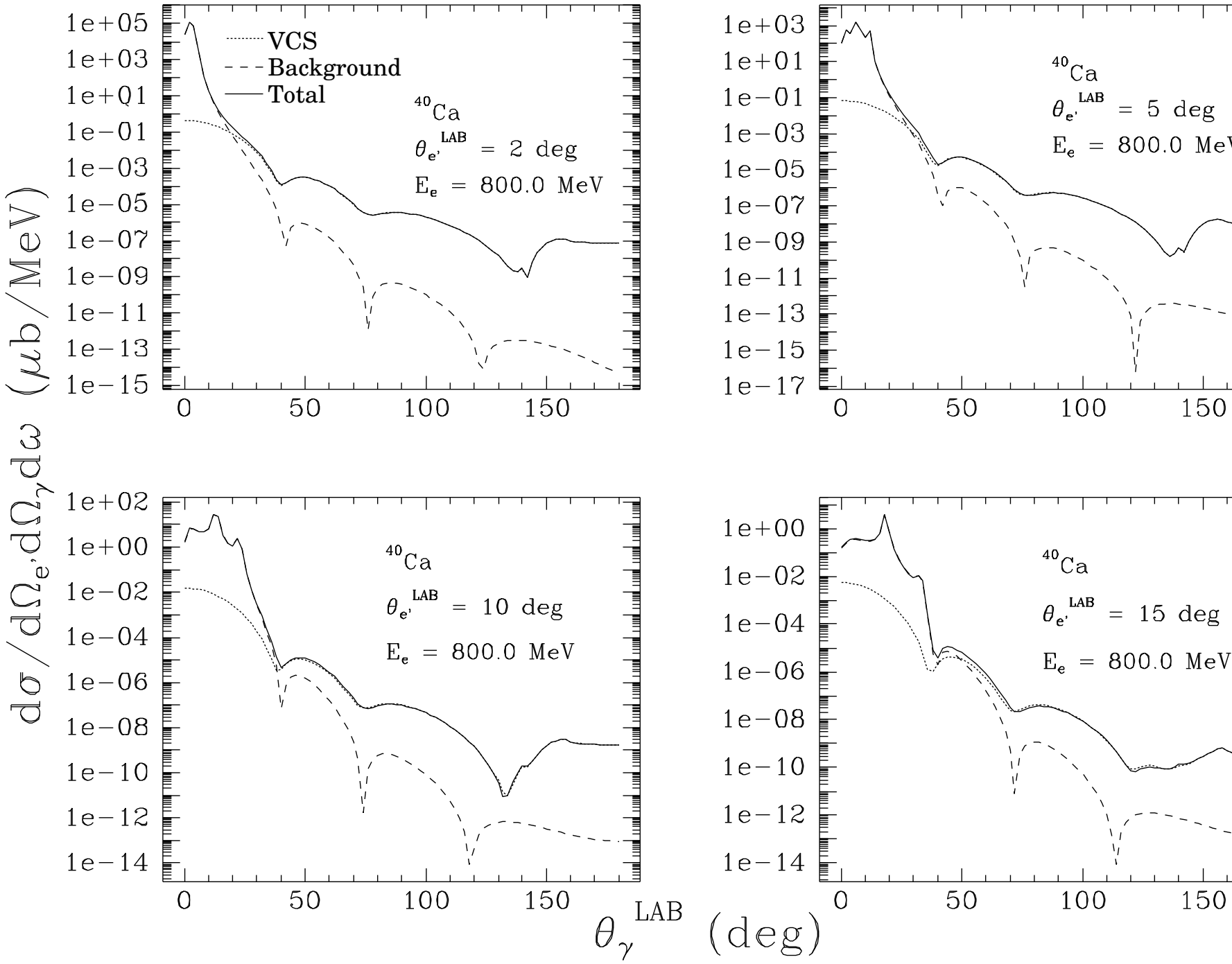
VCS
Background
Total
^{40}Ca
$\theta_{e'}^{LAB}$ = 2 deg
E_e = 800.0 MeV
^{40}Ca
$\theta_{e'}^{LAB}$ = 5 deg
E_e = 800.0 MeV
^{40}Ca
$\theta_{e'}^{LAB}$ = 10 deg
E_e = 800.0 MeV
^{40}Ca
$\theta_{e'}^{LAB}$ = 15 deg
E_e = 800.0 MeV
$d\sigma/d\Omega_{e'}d\Omega_\gamma d\omega$ (μb/MeV)
θ_γ^{LAB} (deg)

Figure 9:

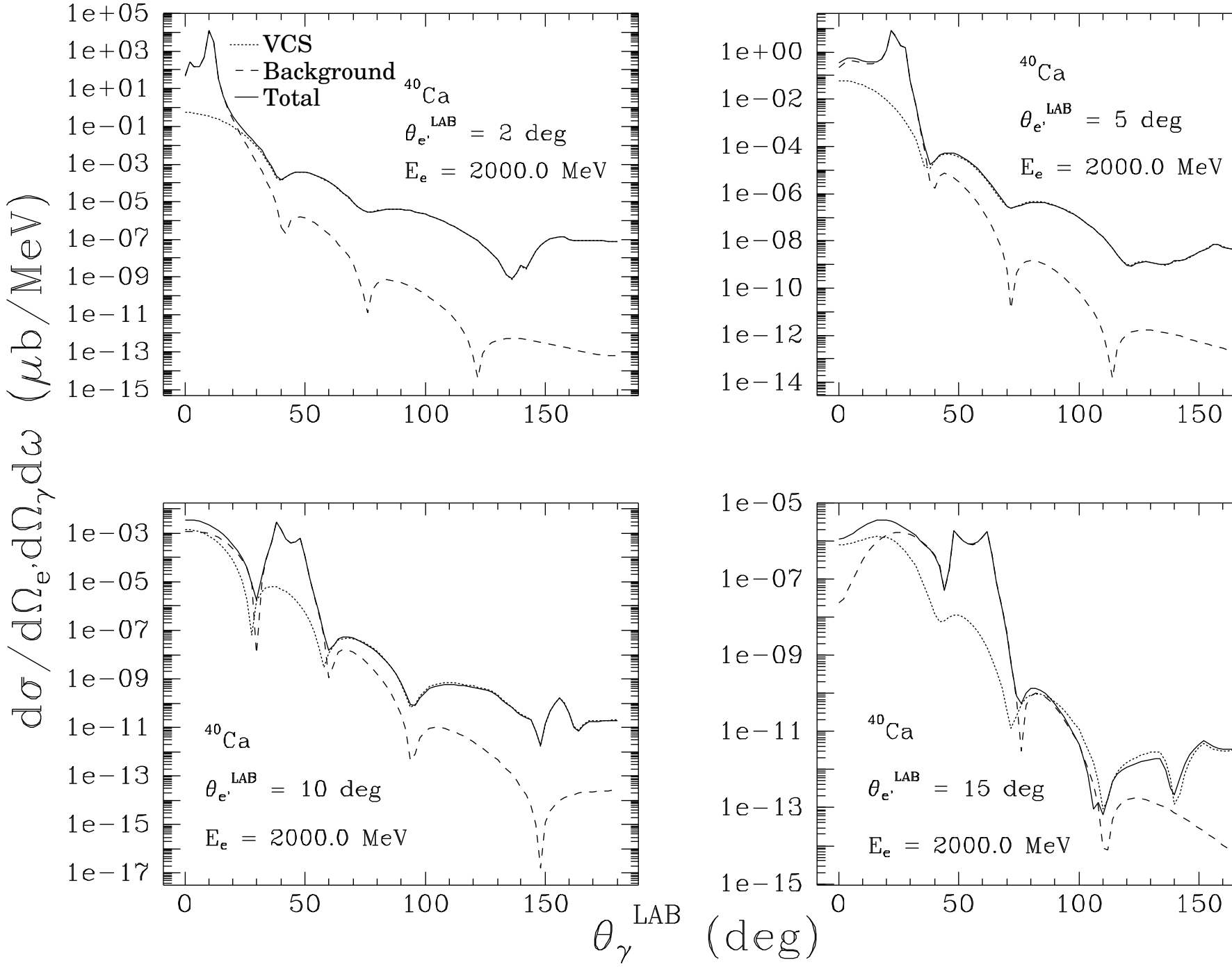
VCS
Background
Total
^{40}Ca
$\theta_{e'}^{LAB}$ = 2 deg
E_e = 2000.0 MeV
^{40}Ca
$\theta_{e'}^{LAB}$ = 5 deg
E_e = 2000.0 MeV
^{40}Ca
$\theta_{e'}^{LAB}$ = 10 deg
E_e = 2000.0 MeV
^{40}Ca
$\theta_{e'}^{LAB}$ = 15 deg
E_e = 2000.0 MeV
$d\sigma/d\Omega_{e'}d\Omega_\gamma d\omega$ (μb/MeV)
θ_γ^{LAB} (deg)

Figure 10:

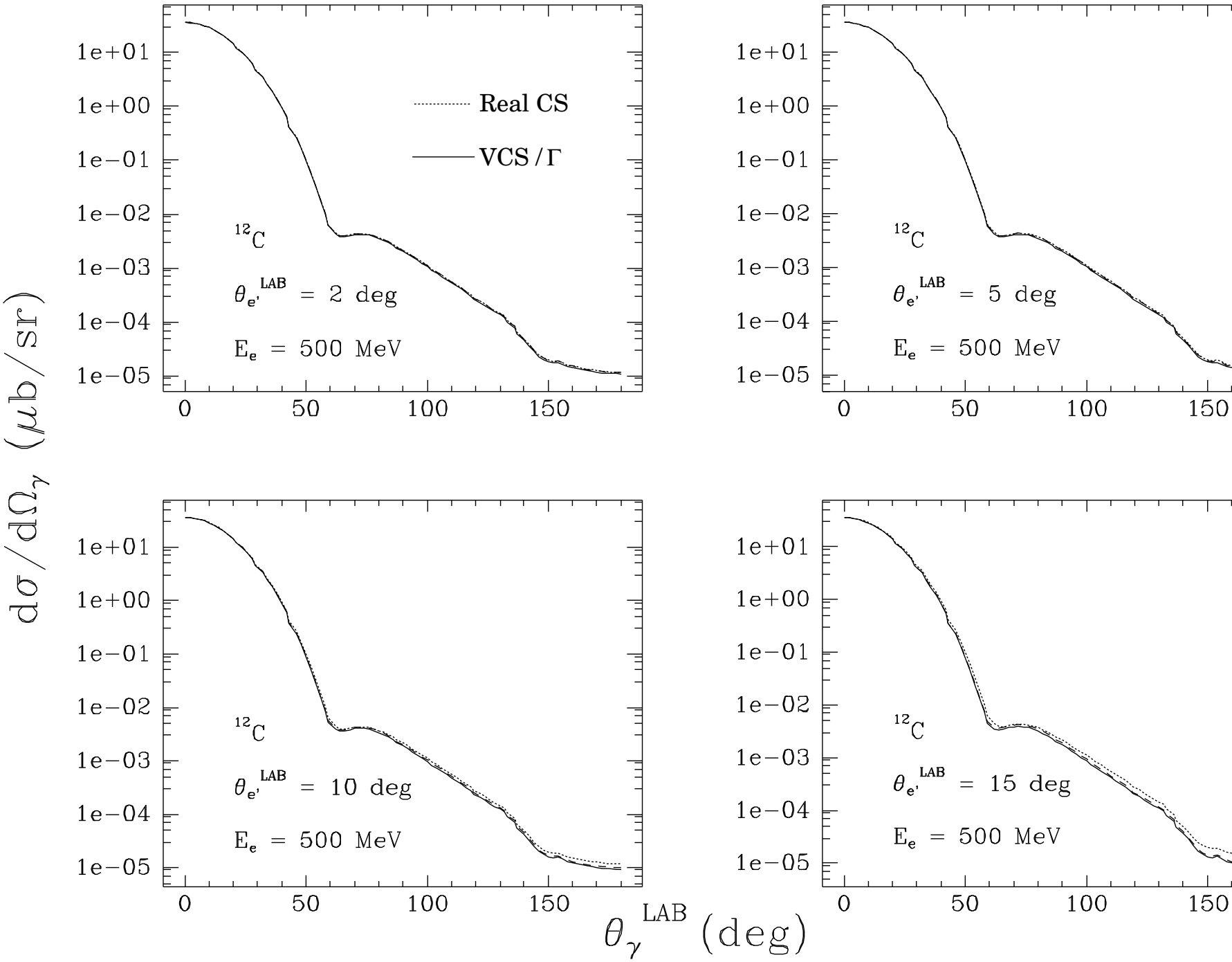
Real CS
VCS / Γ
^{12}C
$\theta_{e'}^{LAB}$ = 2 deg
E_e = 500 MeV
^{12}C
$\theta_{e'}^{LAB}$ = 5 deg
E_e = 500 MeV
^{12}C
$\theta_{e'}^{LAB}$ = 10 deg
E_e = 500 MeV
^{12}C
$\theta_{e'}^{LAB}$ = 15 deg
E_e = 500 MeV
$d\sigma / d\Omega_\gamma$ (μb/sr)
θ_γ^{LAB} (deg)

Figure 11:

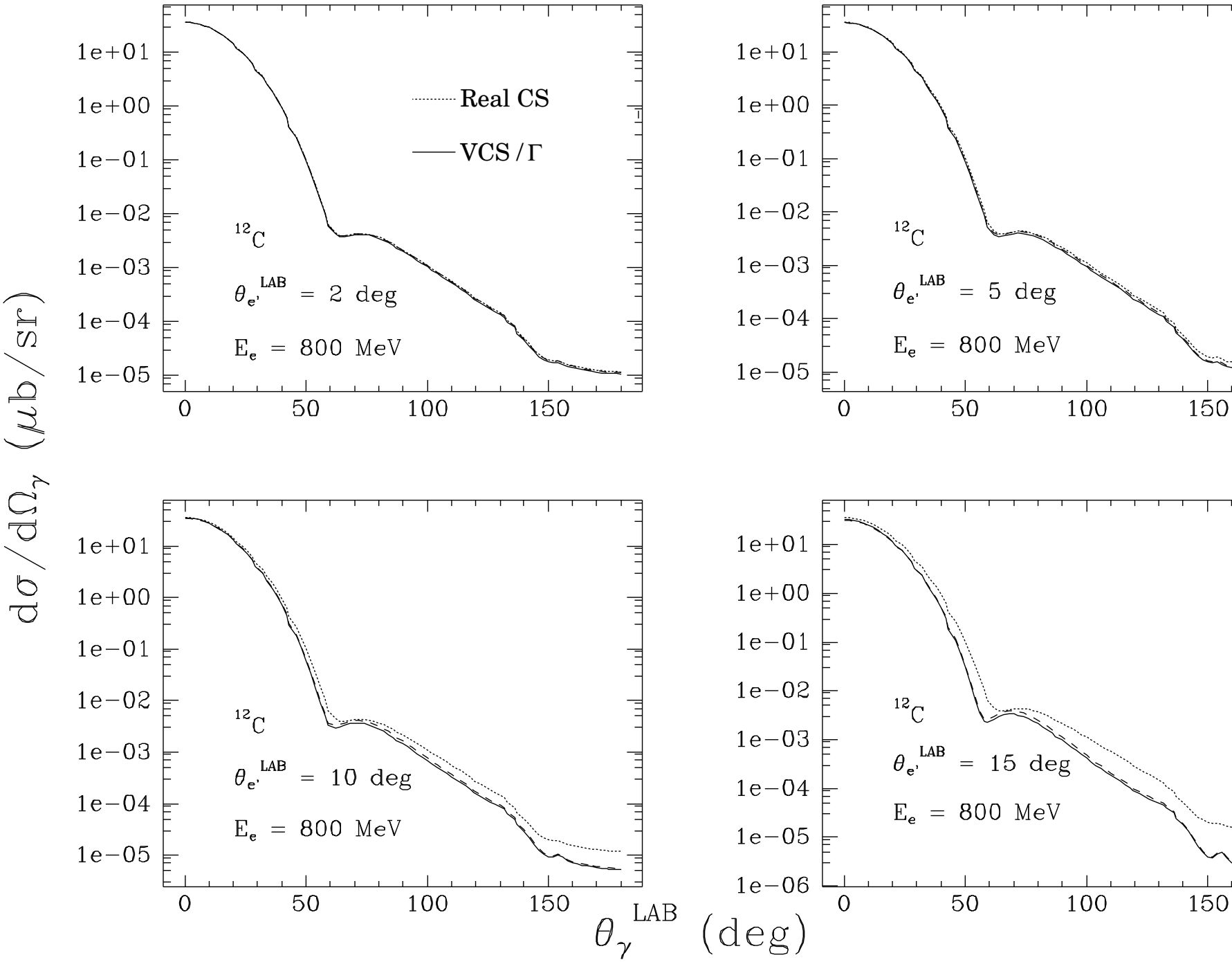
Real CS
VCS / Γ
^{12}C
$\theta_{e'}^{LAB}$ = 2 deg
E_e = 800 MeV
^{12}C
$\theta_{e'}^{LAB}$ = 5 deg
E_e = 800 MeV
^{12}C
$\theta_{e'}^{LAB}$ = 10 deg
E_e = 800 MeV
^{12}C
$\theta_{e'}^{LAB}$ = 15 deg
E_e = 800 MeV
$d\sigma / d\Omega_\gamma$ (μb/sr)
θ_γ^{LAB} (deg)

Figure 12:

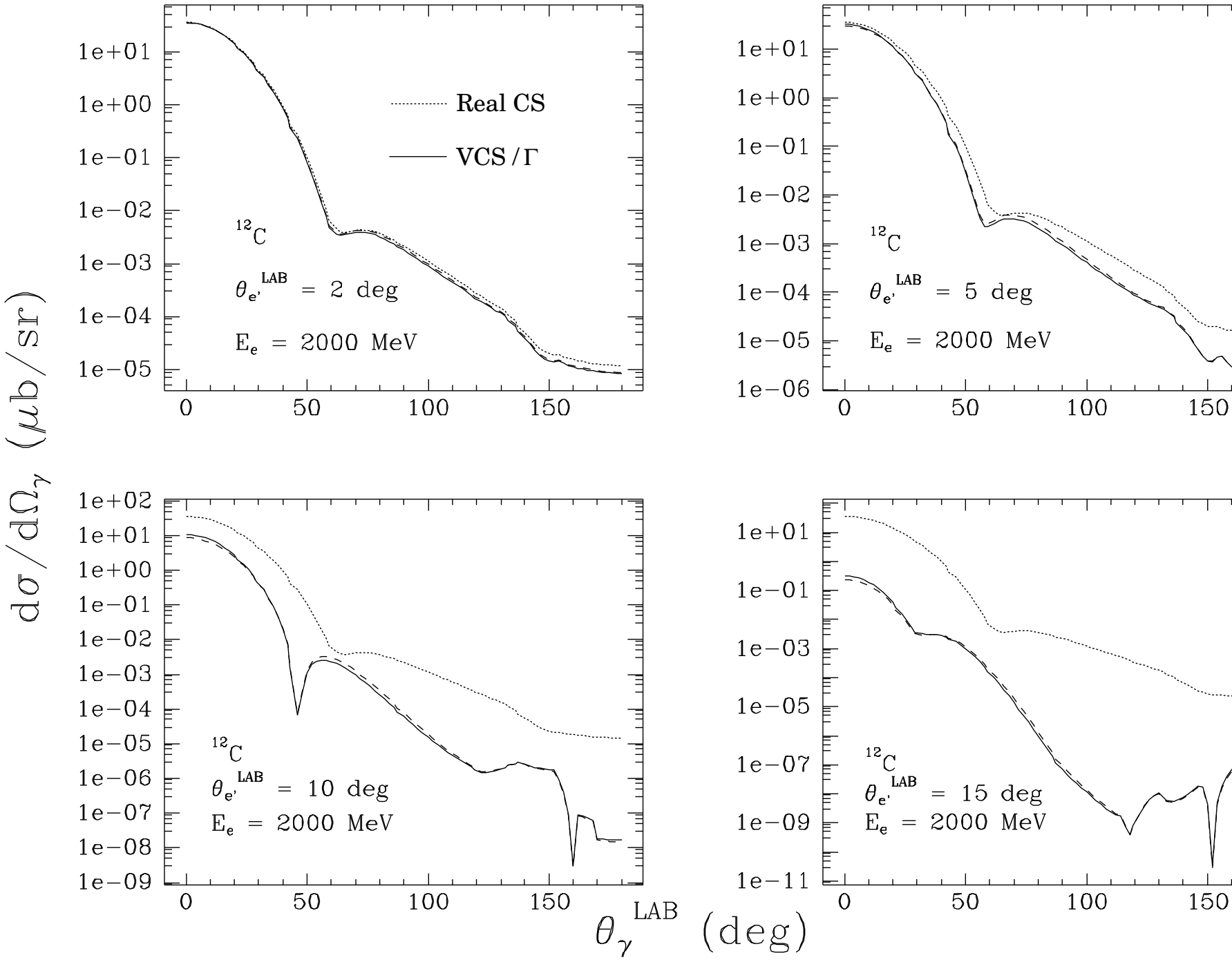
Real CS
VCS / Γ
^{12}C
$\theta_{e'}^{LAB}$ = 2 deg
E_e = 2000 MeV
^{12}C
$\theta_{e'}^{LAB}$ = 5 deg
E_e = 2000 MeV
^{12}C
$\theta_{e'}^{LAB}$ = 10 deg
E_e = 2000 MeV
^{12}C
$\theta_{e'}^{LAB}$ = 15 deg
E_e = 2000 MeV
$d\sigma / d\Omega_\gamma$ (μb/sr)
θ_γ^{LAB} (deg)

Figure 13:

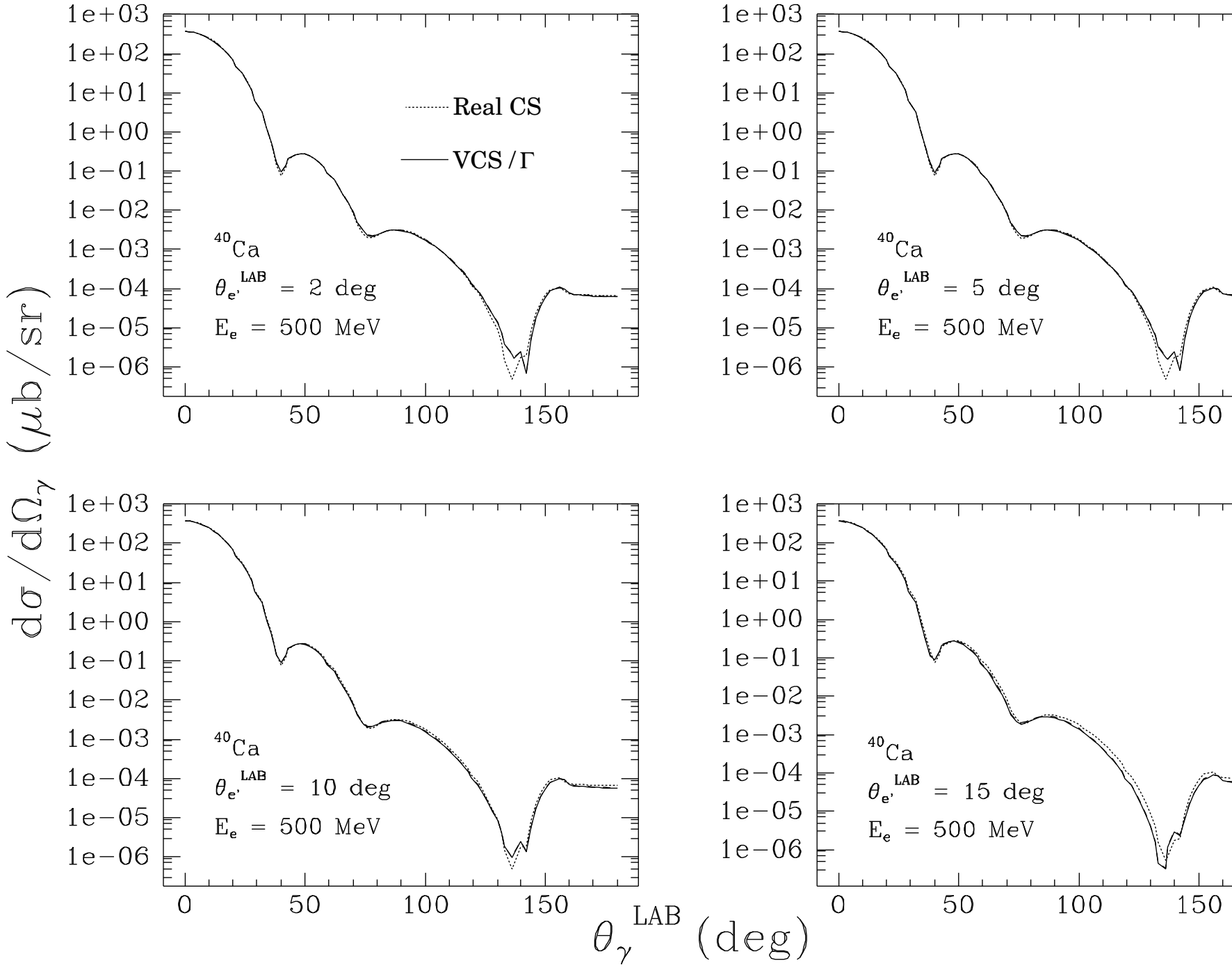
Real CS
VCS / Γ
^{40}Ca
$\theta_{e'}^{LAB}$ = 2 deg
E_e = 500 MeV
^{40}Ca
$\theta_{e'}^{LAB}$ = 5 deg
E_e = 500 MeV
^{40}Ca
$\theta_{e'}^{LAB}$ = 10 deg
E_e = 500 MeV
^{40}Ca
$\theta_{e'}^{LAB}$ = 15 deg
E_e = 500 MeV
$d\sigma/d\Omega_\gamma$ (μb/sr)
θ_γ^{LAB} (deg)

Figure 14:

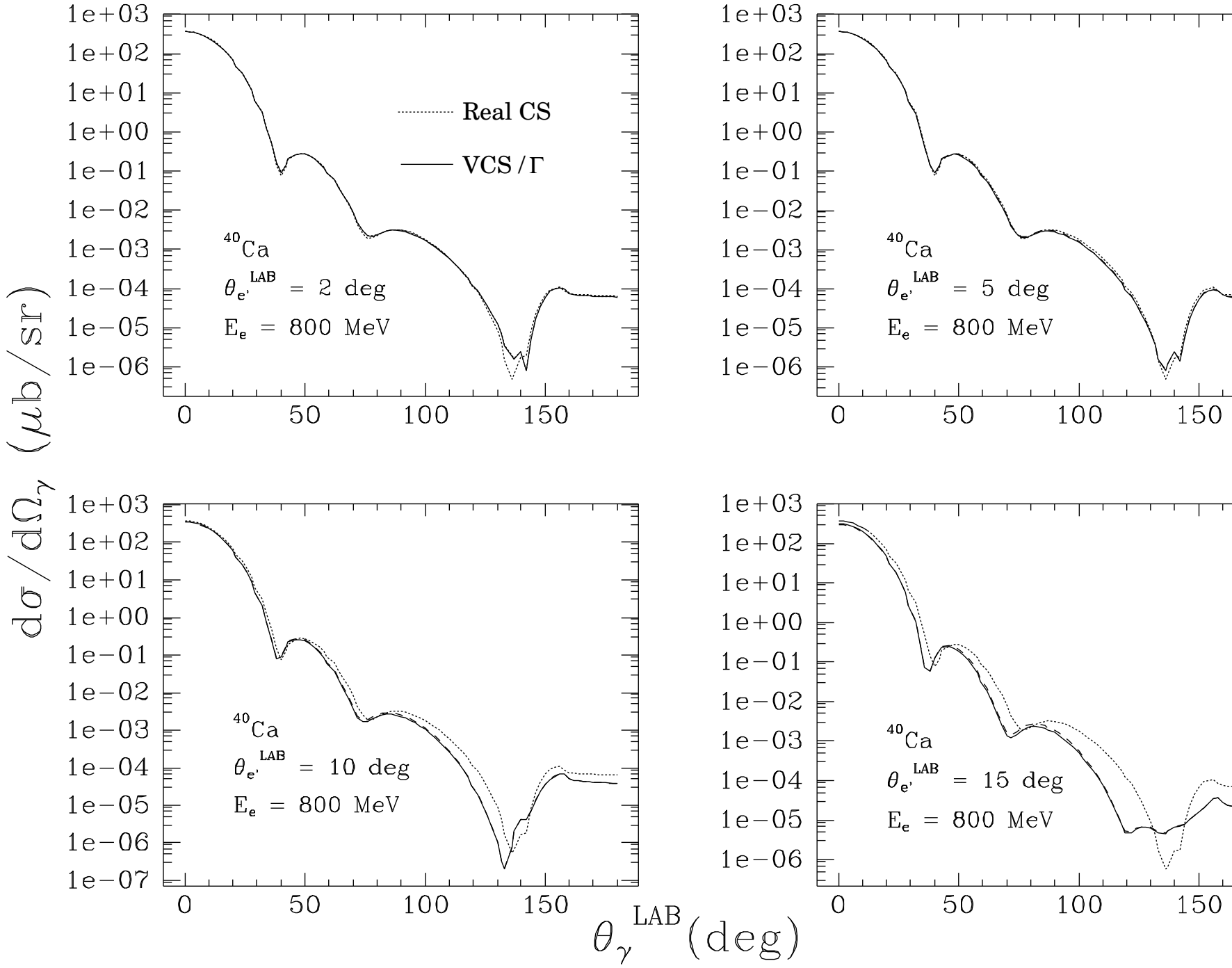
Real CS
VCS / Γ
^{40}Ca
$\theta_{e'}^{LAB}$ = 2 deg
E_e = 800 MeV
^{40}Ca
$\theta_{e'}^{LAB}$ = 5 deg
E_e = 800 MeV
^{40}Ca
$\theta_{e'}^{LAB}$ = 10 deg
E_e = 800 MeV
^{40}Ca
$\theta_{e'}^{LAB}$ = 15 deg
E_e = 800 MeV
$d\sigma / d\Omega_\gamma$ (μb/sr)
θ_γ^{LAB} (deg)

Figure 15:

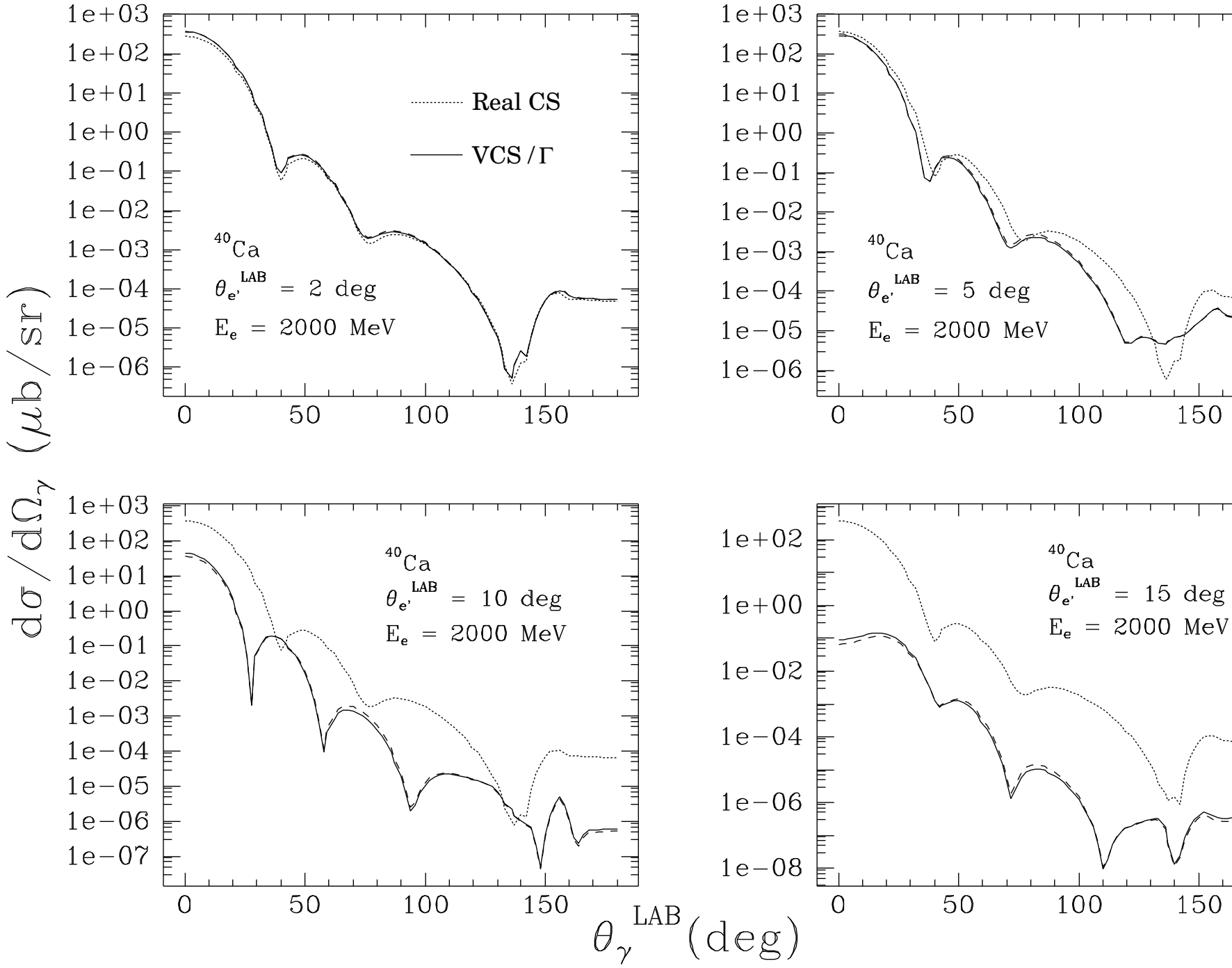
Real CS
VCS / Γ
^{40}Ca
$\theta_{e'}^{LAB}$ = 2 deg
E_e = 2000 MeV
^{40}Ca
$\theta_{e'}^{LAB}$ = 5 deg
E_e = 2000 MeV
^{40}Ca
$\theta_{e'}^{LAB}$ = 10 deg
E_e = 2000 MeV
^{40}Ca
$\theta_{e'}^{LAB}$ = 15 deg
E_e = 2000 MeV
$d\sigma / d\Omega_\gamma$ (μb/sr)
θ_γ^{LAB} (deg)

Figure 16: